Methanol Oxidation on Rhodium As Probed by Surface-Enhanced Raman and Mass Spectroscopies: Adsorbate Stability, Reactivity, and Catalytic Relevance

Christopher T. Williams,[†] Christos G. Takoudis,[§] and Michael J. Weaver*[,‡]

School of Chemical Engineering and Department of Chemistry, Purdue University, West Lafayette, Indiana 47907, and Department of Chemical Engineering, University of Illinois at Chicago, 810 S. Clinton St., Chicago, Illinois 60607

Received: July 18, 1997; In Final Form: November 6, 1997[⊗]

The relationship between surface speciation and catalytic activity/selectivity during methanol oxidation on polycrystalline rhodium under ambient-pressure flow-reactor conditions was studied from 25 to 500 °C by means of surface-enhanced Raman spectroscopy (SERS) along with parallel mass spectrometric (MS) measurements. By utilizing SERS-active Rh films formed by electrodeposition onto gold, the former technique provides in situ surface vibrational spectra with unique sensitivity under these demanding conditions, enabling adsorbed species to be probed in real time (≈1 s) for comparison with the overall kinetics as evaluated by MS. Exposure of Rh to O_2-free methanol yielded no detectable vibrational bands between 25 and 500 °C, although methanol decomposition to form CO and H_2 was evident from MS. The presence of even subunity molar ratios of oxygen, however, yielded rich SER spectra, highlighted by bands indicative of $CO_{(ads)}$ (ν_{Rh-CO} = 465 cm^{-1}, $\nu_{Rh-CO} \approx$ 2000 cm^{-1}). The catalytic selectivity toward CO_2 (versus CO) gaseous product formation decreased markedly around the desorption temperature of $CO_{(ads)}$, ≈ 350 °C under these conditions. This is consistent with the facilitation of CO_2 production by the presence of $CO_{(ads)}$. Complete selectivity toward exhaustive methanol oxidation (i.e., CO_2, H_2O formation) was observed in oxygen-rich methanol mixtures, adsorbed CO now being absent at all temperatures. The CO_2 production occurs partly via methanolic C−O cleavage as deduced by $^{18}O_2$ substitution. The presence of rhodium oxide (Rh_2O_3) was diagnosed for such reactant mixtures above ca. 300 °C from the characteristic 500−580 cm^{-1} ν_{Rh-O} bands. The kinetics of formation and removal of the oxide were probed by gas flow-switching coupled with transient SERS measurements. The oxide formation rates following O_2 exposure are slowed markedly (>100-fold) by the presence of even a small (5%) methanol mole fraction. Switching to pure methanol results in very rapid oxide reduction, so that, for example, removal is complete within ca. 1 s at 350 °C with 100 Torr of CH_3OH. Examination of the transient oxide removal kinetics as a function of temperature and methanol pressure revealed a transition from strongly activated to essentially *T*-independent behavior at lower pressures and/or higher temperatures. This is indicative of a change from rate-determining removal of oxygen from the oxide lattice to a subsequent step involving formation of and/or reaction with an adsorbed methanol scavenger. While such reactivity earmarks the oxide as a potential reaction intermediate, the overall catalytic turnover rates for methanol oxidation are nonetheless faster than can readily be accommodated on this basis.

Introduction

The methanol oxidation reaction over transition-metal catalysts has received much attention over the past decade, due in large part to environmental concerns regarding control of volatile organic compound emissions from industrial processes,[1] as well as automobile emissions standards.[2] The interaction of methanol with these surfaces also affords mechanistic insight into its formation reaction from syngas (i.e., CO, CO_2, H_2). Additionally, the inherent chemical richness present in such a simple molecule has made methanol a prime candidate for more fundamental studies of adsorption, dissociation, and reaction.

One of the transition metals that has exhibited promise for catalytic methanol oxidation is rhodium. The highest pressure (≈0.1 Torr) investigations available have examined the kinetics of both methanol dissociation[3,4] and oxidation[4,5] over polycrystalline[3,4] and supported Rh catalysts.[5] While supported Rh catalysts display some selectivity toward partial oxidation products such as CH_3OCH_3 and H_2CO,[5] exclusive formation of CO_2 and CO is observed over polycrystalline Rh.[4] Several studies have examined adsorption of methanol on clean[6−10] and oxygen-covered[7,10] Rh single-crystal surfaces under ultrahigh-vacuum (UHV) conditions. These show that at low temperatures (<250 K) CH_3OH dissociation proceeds through a stable methoxy ($-OCH_3$) intermediate to form adsorbed carbon monoxide, as evidenced by electron energy loss spectroscopic (EELS) and temperature-programmed desorption (TPD) measurements.[6,7] These observations are similar to those found for other transition metals under comparable conditions.[11] Furthermore, the low desorption temperatures of methanol (≈200 K) and methoxy (≈250 K) from Rh measured by TPD[6,7,10] suggest that the coverages of these species during methanol oxidation at higher temperatures would be small. However, there are no studies in which surface species on Rh have been monitored in situ during reaction of methanol with oxygen at

[†] School of Chemical Engineering, Purdue University.
[‡] Department of Chemistry, Purdue University.
[§] University of Illinois at Chicago.
[⊗] Abstract published in *Advance ACS Abstracts,* December 15, 1997.

S1089-5647(97)02353-5 CCC: $15.00
Published on Web 01/08/1998

higher (up to ambient) partial pressures (i.e., under catalytically relevant conditions). Such information would clearly be invaluable for elucidating the role of adsorbed species in determining overall rates and mechanisms, especially the selectivity toward total and/or partial oxidation products.

We have demonstrated in previous reports[12−14] how surface-enhanced Raman spectroscopy (SERS) can be used as an interfacial vibrational probe of reactive as well as stable adsorbates involved in heterogeneous catalysis on transition metals, including NO reduction by CO over Rh,[13d] Pt,[14b] and Pd[14b] and, more recently, CO hydrogenation on Rh.[14c] The surfaces utilized for these studies were electrochemically deposited transition-metal thin films on roughened SERS-active gold substrates.[15] These films exhibit remarkably stable as well as intense SERS activity, even at elevated temperatures, and largely mimic the adsorptive and catalytic behavior of conventional polycrystalline transition metals. A major virtue of this approach is the ability to monitor adsorbed oxygen and other species from their characteristic surface−adsorbate vibrations, since SERS is sensitive to such modes which appear in the low-frequency (200−1000 cm^{-1}) region that is largely inaccessible to infrared probes. The advent of charge-coupled device (CCD) technology along with the intrinsically intense SERS signals also allows the acquisition of spectral sequences on a rapid ($\approx$1 s) time scale, thereby enabling us to probe the temporal evolution of surface species by perturbing the system parameters (e.g., temperature, reactant ratio) in a gas-flow reactor arrangement and monitoring the transient spectroscopic response. Additionally, kinetic measurements obtained by means of mass spectrometry (MS) allow for direct correlations to be made between overall rates of reaction and surface speciation.[13d,14a−c,e]

Recently, we reported SER spectral evidence of surface oxide formation during methanol oxidation over rhodium.[14d] The ability to detect surface−adsorbate vibrations and the inherent temporal resolution of SERS provides new information regarding the reactivity of lattice oxide (Rh_2O_3) under reaction conditions. This paper expands on that work with a combined SERS and MS investigation of methanol oxidation over polycrystalline rhodium at ambient gas pressures and elevated temperatures. The comparison of observed surface intermediate (e.g., CO,Rh_2O_3) reactivity with overall rates of product (CO_2, CO, H_2O) formation elucidates the mechanistic significance of such adsorbed species under practical reaction conditions. Mechanisms for the formation and removal of lattice Rh_2O_3 are also discussed. A related study of methanol oxidation on palladium will be presented elsewhere.[14e]

Experimental Section

The SERS-active rhodium films were prepared by utilizing 6 mm diameter disks cut out of 0.1 mm thick gold foil (99.95% pure, Johnson Matthey) and polished using 0.3 μm alumina powder. They were then placed into an electrode holder that exposed ca. 0.07 cm^2 of the surface and subjected to oxidation−reduction cycling (ORC) in 0.1 M KCl to produce the surface roughness necessary for Raman enhancement.[15a] The surface was rinsed thoroughly with deionized water and subsequently transferred to another cell for electrochemical deposition of the Rh overlayers. The procedure for Rh deposition utilized a 0.3 mM solution of $RhCl_3$ in 0.1 M $HClO_4$ at 0.1 V vs SCE. The cathodic charge was monitored and controlled in order to limit the deposition to the desired film thickness, usually between 2 and 5 equivalent monolayers.[15b,c] This choice of film conditions has been found to optimize the SER spectral behavior in both gas-phase[14] and electrochemical[15b,c] environments.

The reactor utilized for the SERS experiments consists of a 100 cm^3 six-way cross, equipped with a turbomolecular pump (Balzers TPH 060) yielding a base pressure of 10^{-6} Torr. A combination of needle, gate, and butterfly valves allows operation of the reactor at pressures ranging from 10^{-3} to 760 Torr. The pressure over the entire range is measured using a combination of Pirani and cold-cathode gauges (Balzers PKR 250), controlled by a Balzers TPG 252 pressure controller. One of the reactor arms contains an optical viewport, over which the specimen is mounted on a stainless steel cylindrical sample holder which can be heated to 500 °C. Inside the sample holder, a solid piece of stainless steel is surrounded by a coil of thin Nichrome wire to provide resistive heating. Through the center of this heater is a K-type thermocouple which is in intimate contact with the sample and leads to a programmable temperature controller (Omega CN2041). Laser excitation at 647.1 nm is provided by a Kr^+ laser (Spectra Physics), and scattered light is collected by a three-stage spectrometer (SPEX Triplemate), equipped with a liquid nitrogen-cooled Photometrics CCD. The (room temperature) gaseous reactants are introduced into the reactor through a manifold that allows mixing of up to four inlet gases; flow rates are measured with a bubble flow meter. Recent reactor modifications allow introduction of such reaction mixtures nearer to the sample as well as provide efficient ($\leq$5 s) mixing characteristics required for analysis of transient spectral response experiments. Methanol was introduced into the reactor by bubbling Ar through the liquid phase, thereby saturating the flowing room-temperature gas. Various reactant ratios were achieved by subsequently mixing the resulting stream with oxygen and/or argon. The reactants utilized were 99.9% pure MeOH (Fisher) and gases of ultrahigh-purity grade (Airco). Isotopically labeled compounds were obtained from Cambridge Isotope Laboratory (98% pure $^{18}O_2$, 99% pure ^{13}CO, 99% pure CH_3OD, 99.8% pure CD_3OD) and used without further purification.

As the surface area of the substrate utilized for SERS was too small (0.07 cm^2) to yield reliable kinetic data, larger surface area variants were prepared. These consisted of 5 m long, 0.05 mm diameter gold wires (99.998% pure, Johnson Matthey) that were subjected to the same oxidation−reduction cycling and Rh deposition procedure described above. This provided catalysts with a larger (ca. 7 cm^2) surface area and yet having the same film morphology as the SERS-active foils. The catalyst was placed on a resistively heated sample holder, and a K-type thermocouple was used to measure catalyst temperature. The kinetic experiments were carried out in a small-volume (ca. 4 cm^3) stainless steel flow reactor (Spectra-Tech) that could be evacuated to 10^{-6} Torr via a turbo pump (Balzers). Gas-phase composition was measured by leaking the gas outlet into a Lybold Inficon IPC-50 quadrupole mass spectrometer.

Results and Discussion

The surfaces were pretreated by heating to 150 °C in 100 cm^3 min^{-1} of H_2 for about 5−10 min. This procedure resulted in a clean SERS background in the 200−1000 cm^{-1} range but retained weak features in the 1300−1600 cm^{-1} region due to surface carbonaceous residues. Complete removal of these bands required prior high-temperature oxidation, which typically resulted in severe disruption of the film and substantial loss of SERS activity following reduction with H_2; this was therefore not used as part of the pretreatment procedure. Following the H_2 pretreatment, the sample was cooled to 100 °C and the reactor flushed out with Ar prior to adding reactive gas mixtures. Identical pretreatment procedures were utilized during both SERS and MS experiments described below.

The various experimental tactics, as reflected in the ensuing presentation, were as follows. Prior to investigating the state of the surface under reaction conditions, it is desirable to first obtain SER spectra during heating in each of the reactants separately. Subsequently, progress of the reaction in two distinctly different gas mixtures, specifically excess methanol and excess oxygen, in argon was probed in combined fashion by SERS and MS. The general procedure followed was similar to that used in our recent study of CO hydrogenation on Rh.[14c] During SERS experiments the 0.07 cm^2 catalysts were exposed to each reactant mixture and heated in a stepwise periodic fashion, waiting at each temperature for a time-independent response to be attained (ca. 3 min) before spectra were finally recorded. Using an identical heating procedure under the same conditions, the catalytic activity of the higher surface area Rh catalysts (vide supra) in the smaller volume reactor was examined by monitoring gas-phase product formation with mass spectrometry. A series of *m*/*e* values were monitored that encompassed the wide range of possible products, with data acquired continuously and recorded every 3 s. With *m*/*e* values listed in order of decreasing intensity, these included CO_2 (44, 16, 28, 12), CO (28, 12, 16), H_2O (18, 17, 16), H_2 (2), CH_2O (29, 30, 28), and CH_3OCH_3 (46), as well as the reactants, CH_3OH (31, 32, 29, 28) and O_2 (32, 16).

Several transient experiments were also performed involving the monitoring of surface changes with SERS during step changes in reactor compositions. These were designed to probe further the reactivity of adsorbates observed under steady-state reaction conditions. As we have shown in previous studies, these approaches assist in elucidating the kinetics of various surface processes, as well as delineate their probable importance in the reaction mechanism.[13e]

Oxygen Adsorption. The interaction of oxygen on Rh at ambient pressures (0.3 atm) and elevated temperatures (25−300 °C) has been previously examined by Tolia et al.[13c] using SERS together with X-ray photoelectron spectroscopy (XPS). A Raman band at 530 cm^{-1} was observed at elevated temperatures (>150 °C) along with a second, behaviorally distinct, feature at 290 cm^{-1}. The 530 cm^{-1} band was assigned to the ν_{Rh-O} symmetric stretch of Rh_2O_3 based on comparisons with Raman spectra of bulk oxide and correlations with parallel XPS data. More recent observation of the expected ca. 20 cm^{-1} downshift upon substitution with ^{18}O confirms that the species responsible for the 530 cm^{-1} feature is formed from O_2.[14c] While assignment of the 290 cm^{-1} band was more challenging, a similar feature was observed during our recent study of CO hydrogenation over Rh.[14c] Based on its unusual stability under reducing conditions and an observed 15 cm^{-1} downshift upon substitution with $^{18}O_2$, the feature was assigned to subsurface oxygen.

While the interaction of oxygen with Rh[16−18] and the subsequent surface oxidation process[13c,19] have been the subject of numerous investigations, most have involved ex situ analysis of oxide films in UHV.[16−19] As a result, there is a paucity of kinetic information regarding the initial formation of surface oxide at ambient pressures. Given our observation of Rh_2O_3 formation during methanol oxidation (vide infra),[14d] the kinetics of Rh surface oxidation were probed utilizing transient spectral tactics. These entailed monitoring the temporal evolution of Rh_2O_3 (ν_{Rh-O} = 530 cm^{-1}) with SERS during exposure of Rh to a range of O_2 partial pressures (7.6−760 Torr) at various temperatures (350−500 °C). Samples were first heated in vacuum to the temperature of interest, at which point an oxygen/argon mixture containing the desired O_2 partial pressure was flushed into the reactor. This protocol essentially instantaneously (<1 s) exposes the surface to the given mixture, thus negating the effects of reactor mixing time. Figure 1 shows a typical sequence of SER spectra obtained at the times indicated following addition of a 100 cm^3 min^{-1} flow of pure O_2 at 1 atm and a surface temperature of 450 °C. The spectra were recorded utilizing a 0.5 s acquisition time, which is the minimum required to achieve an acceptable signal-to-noise ratio. Rhodium oxide formation is seen to be completed even within the first 0.5 s following O_2 exposure, as evidenced by the appearance of the Raman band at 530 cm^{-1} and its unchanged appearance in the subsequent spectra (Figure 1). Identical results were obtained for the other conditions examined (350−450 °C and 7.6−760 Torr of O_2). Thus, the rate of oxide formation was too fast to measure given the temporal resolution of our spectrometer/CCD system.

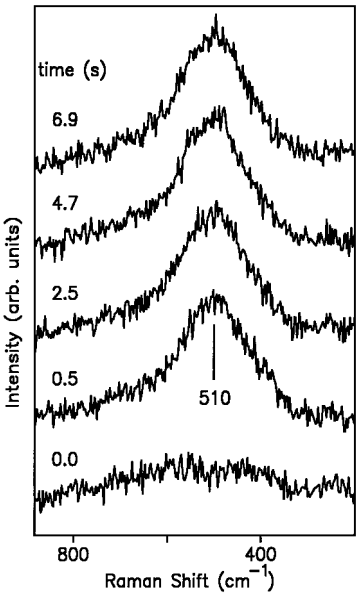

Figure 1. Transient SER spectra following exposure of a reduced Rh surface to a 100 cm^3 min^{-1} flow of pure O_2 at 1 atm and 450 °C. The surface was first heated in vacuum to 450 °C followed by instantaneous (<1 s) exposure at $t = 0$ s. The spectral acquisition time was 0.5 s; the times indicated are "average" values during each spectral acquisition following O_2 exposure.

These findings are consistent with those of Kellogg, who investigated Rh_2O_3 formation kinetics during the initial stages of surface oxidation with imaging atom-probe mass spectrometry and field ion microscopy.[19] Initial lattice oxide formation rates were obtained by measuring the oxygen uptake of the Rh field emitter tip as a function of exposure time at various temperatures and O_2 partial pressures (0.1−1 Torr). Oxide growth proceeded initially at a rate of ca. 3−5 layers s^{-1}, with a preexponential factor of 70 layers s^{-1} and an activation energy of 3−4 kcal mol^{-1}. Therefore, it is unsurprising that the oxide formation in the present case is complete within the first 0.5 s following O_2 exposure, especially given that we are examining only ca. 4 rhodium monolayers. Kellogg also noted that the initial oxidation rate was nearly independent of pressure over the limited range examined. Considering that the experiments are performed well below reported desorption temperatures of oxygen from Rh,[16−18] the surface presumably becomes saturated with adsorbed oxygen rapidly. Consequently, the initial rates of surface oxidation are likely to be limited by surface oxidation kinetics rather than the dissociative chemisorption of oxygen,[19c] accounting for the near-independence of the formation kinetics on O_2 pressure as well as their rapidity.

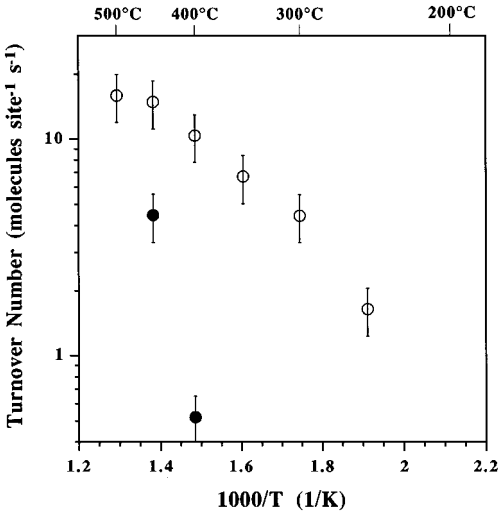

Figure 2. Arrhenius plot of CO formation kinetics obtained following exposure of Rh to 250 cm^3 min^{-1} of 15% CH_3OH/85% Ar at 1 atm total pressure. Rates, obtained by MS measurements, are expressed as turnover numbers. Open and filled symbols refer to rate measurements obtained during stepwise heating and subsequent cooling segments, respectively. (See text for details.)

Methanol Decomposition. Exposing a reduced Rh surface to a range of methanol partial pressures (20−100 Torr) between 100 and 500 °C yielded no discernible SERS features. However, mass spectral measurements conducted under these conditions detected the methanol decomposition products CO and H_2 beginning at ca. 250 °C. For example, Figure 2 shows the Arrhenius plot extracted from the CO production rates (molecules $site^{-1}$ s^{-1}) obtained by heating Rh in 250 cm^3 min^{-1} of 15% CH_3OH/85% Ar at 1 atm. All turnover numbers represent average values over several experiments and were calculated assuming 1.8×10^{15} sites cm^{-2}. The open circles indicate the rates measured during the stepwise heating procedure described above. The observed product formation is qualitatively similar to reports by Schmidt and co-workers of methanol dissociation on polycrystalline Rh at lower pressures (ca. 0.01−0.2 Torr).[3,4] However, while no catalyst deactivation is observed by the latter authors at lower pressure,[3,4] a marked decrease (≈90%) in CH_3OH dissociation was observed in the present case, shown by the depressed CO production rates measured at lower temperatures following excursions up to 500 °C (Figure 2, solid circles). Indeed, high-temperature (ca. 300−400 °C) O_2 oxidation and H_2 reduction was required to restore catalyst activity after such experiments.

Oxidation: Methanol-Rich Conditions. We next consider temperature-dependent SERS and MS data obtained under reaction conditions, initially in the presence of a molar excess of methanol. Unlike the pure methanol case, the presence of some oxygen induced rich SER spectra.

Typical spectra for a reduced Rh surface heated in a 10% O_2/13.5% CH_3OH/76.5% Ar mixture at 1 atm total pressure are presented in Figure 3A,B. Data within the two spectral regions shown (ca. 200−800 and 1800−2300 cm^{-1}, respectively) were obtained separately in order to achieve satisfactory frequency resolution. After exposing the catalyst to the reaction mixture at 100 °C a feature at 250 cm^{-1} was observed, accompanied by a weak 465 cm^{-1} band situated on a broad sloping baseline (Figure 3A). As the temperature was raised to 200 °C, the background diminished to reveal a weak band at ca. 640 cm^{-1}, while the intensity of the 250 and 465 cm^{-1} features increased. At 300 °C, these remaining features began to weaken, with complete removal of the 465 and ca. 640 cm^{-1} bands occurring by 400 °C (Figure 3A). Vestiges of the 250 cm^{-1} feature, however, remained even up to 500 °C. The high-frequency spectra (Figure 3B) revealed a single 1990 cm^{-1} band present at 100 °C, which increased in intensity and upshifted to 2020 cm^{-1} as the temperature was raised to 200 °C. Further heating resulted in the diminution of this feature beginning at 300 °C, with eventual removal by ca. 400 °C.

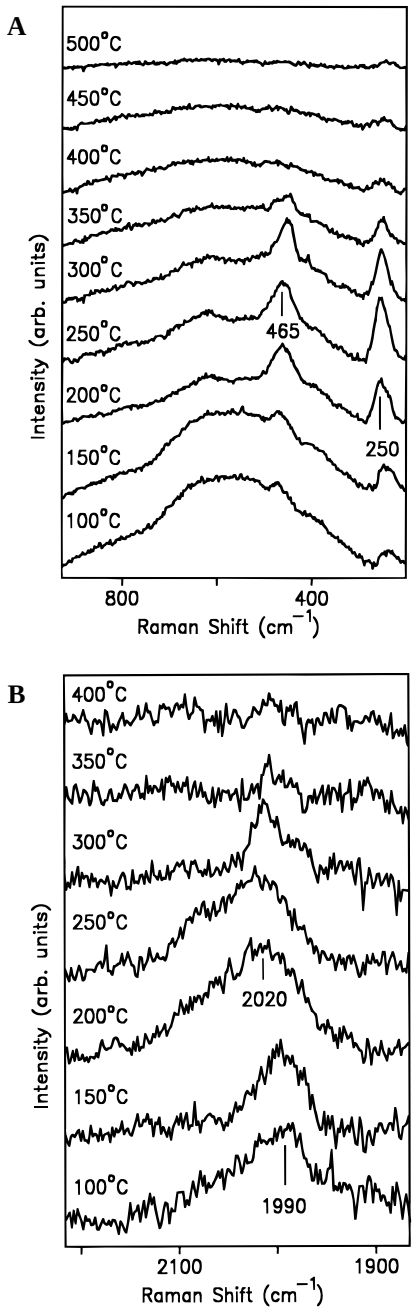

Figure 3. (A) Low-frequency temperature-dependent SER spectra obtained during exposure of Rh to 100 cm^3 min^{-1} of 10% O_2/76.5% Ar/13.5% CH_3OH at 1 atm total pressure. The spectral acquisition time was 20 s. (B) As for (A) but for the high-frequency region and using a spectral acquisition time of 40 s. (See text for details.)

Arrhenius plots extracted from steady-state rate measurements by means of MS are presented in Figure 4. Both CO_2 and CO products were detectable by 200 and 250 °C, respectively, with the carbon balance closing to within 10%. Furthermore, H_2 was found to be the only hydrogen-containing product. The activation energies for CO_2 and CO formation are 12 ± 1 and 8 ± 1 kcal mol^{-1}, respectively, up to 350 °C. In contrast to

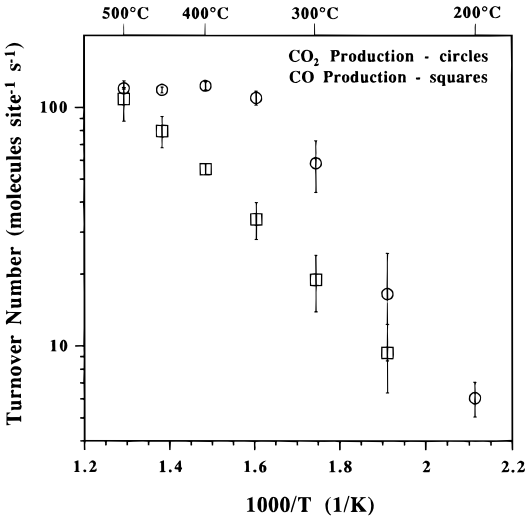

Figure 4. Arrhenius plot of CO_2 and CO formation rates during exposure of Rh to 250 cm^3 min^{-1} of 10% O_2/76.5% Ar/13.5% CH_3OH at 1 atm total pressure. See Figure 2 caption and text for further details.

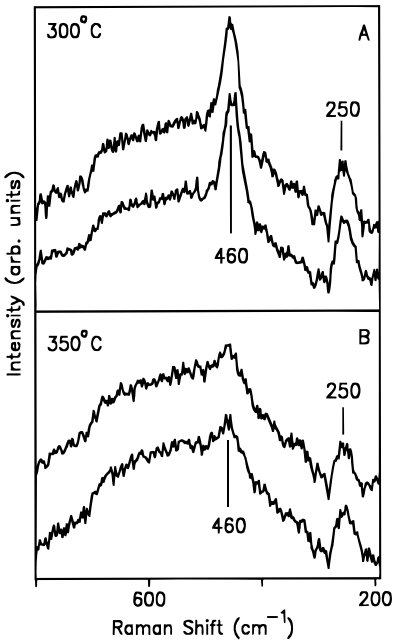

Figure 5. (A) SER spectra of a Rh surface at 300 °C before (bottom spectrum) and 10 min after (top spectrum) switching from a 10% O_2/76.5% Ar/13.5% CH_3OH mixture to 200 cm^3 min^{-1} of pure Ar at 1 atm. The spectral acquisition time was 20 s. (B) As for (A) but at 350 °C.

the results for pure methanol (Figure 2), no significant hysteresis in catalytic activity was observed during increasing and decreasing temperature segments. Comparison of the formation kinetics of the methanol decomposition product CO in the presence (Figure 4) and absence (Figure 2) of oxygen is complicated by catalyst deactivation in the latter case. Nonetheless, the rates in the former appear to be significantly (ca. 5-fold) larger. This difference may be due partly to the ability of O_2 to remove adsorbed carbonaceous impurities and other carbon-containing inhibitors. Such "surface self-cleaning" is probably also responsible for the absence of temperature hysteresis for the kinetics in the O_2-containing case.

To assign the observed SER spectral features in Figure 3A,B, it is useful to make comparisons with earlier vibrational investigations of methanol and CO adsorption on Rh. Previous SERS studies of CO adsorption on Rh revealed two bands at 470 and 2040 cm^{-1} which were assigned to the ν_{Rh-CO} and ν_{C-O} stretching vibrations, respectively, of terminally bound CO.[12a,13a,b,14c] Related EELS studies of methanol adsorption on Rh(100)[6] and Rh(111)[7] also reveal that the only stable carbon-containing species above 25 °C was adsorbed CO, diagnosed by the appearance of 470 and 2050 cm^{-1} bands while heating a methanol adlayer in UHV. Based on these and the above similarities, the present 465 and ca. 2000 cm^{-1} bands are also assigned to stretching vibrations involving CO bound on atop sites. Consequently, the interaction of oxygen with methanol facilitates the dissociation of the latter to form adsorbed CO. Such a phenomenon has been observed previously in UHV[7,10,11a] and will be discussed in more detail below.

The origin of the 250 cm^{-1} feature was probed by substituting $^{18}O_2$, CH_3OD, or CD_3OD into the reactive gas mixture. The absence of a ca. 15 cm^{-1} downshift while substituting $^{18}O_2$ discounts an oxygen species formed by oxidation with the reactant as being responsible for this vibration. Similarly, the lack of a frequency downshift when utilizing the deuterium-labeled methanol suggests that the surface lead-in atom is most likely the carbon or oxygen from methanol. While adsorbed methoxy intermediates have exhibited similar Rh−O stretches in UHV studies, these species were found to decompose below 25 °C.[6,7] The partial stability of the present 250 cm^{-1} feature even up to 500 °C therefore undermines this possibility. Thus, we refrain from a specific assignment of this band and attribute it merely to a species formed from methanol dissociation. While the broad ca. 640 cm^{-1} band appears to be consistent with an O−C−O bending mode of adsorbed formaldehyde,[7] we have observed a somewhat similar feature, assigned to CO_3, during exposure of a Rh surface to CO and O_2.[14c]

The observed desorption temperature of CO (Figure 3) is ca. 100 °C higher than that found during a previous SER study of the adsorbate formed on Rh from gaseous CO.[14c] Furthermore, TPD studies of CO formed from simple adsorption[20] and methanol dissociation[6−10] on Rh in UHV environments both revealed lower desorption temperatures (between 200 and 250 °C). Carbon monoxide desorption temperatures from Rh have, however, been found to increase as surface coverage decreases[20] and may be affected by environmental (i.e., coadsorbate) factors, possibly explaining the increased stability of this moiety in the present case. Indeed, the C−O stretching vibration at ca. 2000 cm^{-1} (Figure 3B) is substantially downshifted (ca. 40 cm^{-1}) from that observed in the case of a pure CO-saturated surface,[14c] suggesting that one or both of these effects are likely occurring.

Given that this unusually stable adsorbed CO is present under reaction conditions (Figure 3), its reactivity is interesting to probe by transient experiments. These involved switching the gas flow from the methanol-rich reaction mixture to pure argon or one of the reactants while simultaneously monitoring the SER spectral changes. Figure 5A shows the results of switching at 300 °C from the reactor containing the 10% O_2/13.5% CH_3OH/76.5% Ar mixture at 1 atm to 200 cm^3 min^{-1} of Ar. The bottom spectrum was taken at $t = 0$ s, while the top spectra was acquired 10 min after the switch. No changes in the Raman intensities were observed, indicating that both the adsorbed CO and 250 cm^{-1} methanol-related moiety are extremely stable on the surface at this temperature. Similar results were found for identical experiments performed at 350 °C (Figure 5B). However, heating the surface to 400 °C in each of the above cases resulted in severe attenuation of both Raman bands, similar to the behavior observed under reaction conditions (Figure 3A). Identical results were obtained upon switching to mixtures containing CH_3OH in argon.

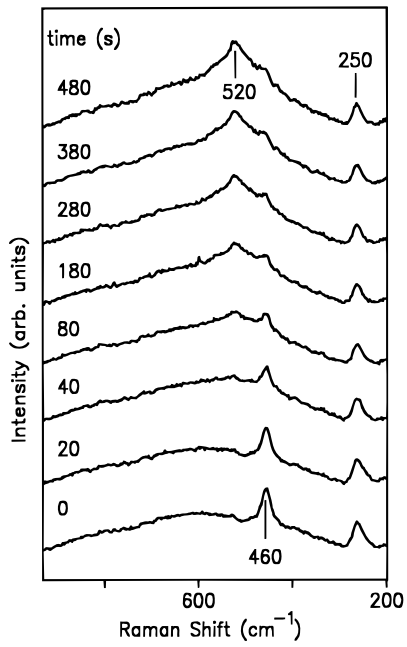

Figure 6. Real-time SER spectra of a Rh surface that was initially held at 250 °C in 100 cm^3 min^{-1} of a 10% O_2/76.5% Ar/13.5% CH_3OH mixture at 1 atm. The flow was then switched to Ar for several minutes, followed by introduction of 200 cm^3 min^{-1} pure O_2 at $t = 0$ s. Subsequent SER spectra were recorded at 20 s intervals at the times indicated with a spectral acquisition time of 20 s.

In contrast, exchanging the reaction mixture with pure oxygen produced a marked change in the SER spectral response. Typical SER spectra acquired during such a procedure at 250 °C are shown in Figure 6. The Rh surface was heated in 10% O_2/13.5% CH_3OH/76.5% Ar to 250 °C and the flow changed to pure Ar, resulting in Raman features similar to those observed above (cf. Figure 3). At $t = 0$ s (bottom spectrum) the flow was changed to 200 cm^3 min^{-1} of O_2, and SER spectra were acquired continuously utilizing a 20 s integration time. A portion of the adsorbed CO is seen to be removed by ca. 80 s, with no subsequent change occurring in the band intensity. The 250 cm^{-1} methanol feature remained unaffected even after 8 min (top spectra). Surface oxide formation ($\nu_{Rh-O} = 520$ cm^{-1}) was also observed beginning at 40 s, the band intensity increasing until ca. 180 s.

Taken in concert with the steady-state SERS and MS measurements (Figures 3 and 4), the results of this and the previous (Figure 5) transient experiments suggest that the adsorbed CO *is largely unreactive* during CH_3OH oxidation to CO_2. A similar deduction applies to the species responsible for the 250 cm^{-1} band. Also interesting is that the rate of oxide formation in Figure 6 is at least 2 orders of magnitude slower than observed upon O_2 exposure in the absence of methanol (Figure 1). One likely factor inducing this inhibition is the significant amount of adsorbed CO and other chemisorbates on the surface. At least partial oxidative removal of the adsorbed CO (Figure 6) is apparently necessary before extensive surface oxidation can proceed.

In light of these findings, it is interesting to see whether correlations can be found between the presence of adsorbed CO and the selectivity toward the formation of CO versus CO_2 gaseous products. Figure 7A shows the temperature-dependent changes in relative coverages of CO (465 cm^{-1}) and the reaction selectivity for the experiments shown in Figures 3 and 4. The relative CO coverage was estimated by normalizing the 465 cm^{-1} band intensity to the maximum value (Figure 3A). The

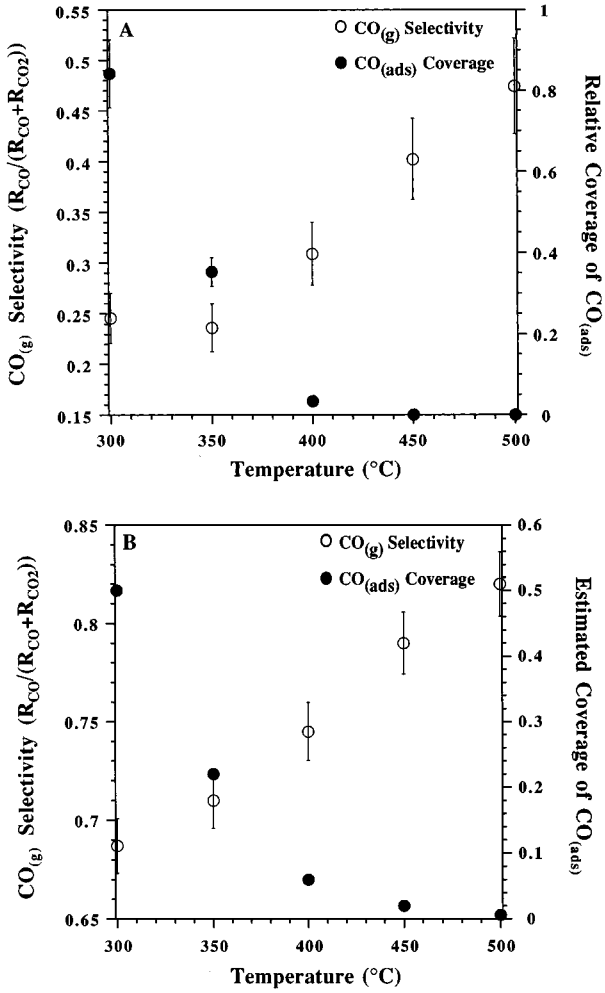

Figure 7. (A) Plot of selectivity toward gaseous CO product formation (open circles) and relative CO coverage (filled circles) as a function of temperature as extracted from the data shown in Figure 2. Coverages, as deduced from SERS intensities (see text), are normalized to the maximum (i.e., initial) values (see text for further details). (B) Corresponding plot of CO selectivity and estimated CO coverage reported in ref 4 for an equimolar mixture of CH_3OH and O_2 at 0.2 Torr total pressure on polycrystalline Rh.

validity of this approach rests on the assumption that the SERS band intensities can vary roughly linearly with surface concentration, a circumstance which has been verified for several other simple metal−adsorbate vibrations.[21] A rough correlation is observed in Figure 7A in that the reaction selectivity toward CO production increases in tandem with the depletion of adsorbed CO. This suggests that the oxidation of methanol to form CO_2 is facilitated by the presence of adsorbed CO; conversely, as the adsorbed CO becomes less stable, it is increasingly likely to escape as gaseous CO rather than become oxidized prior to desorption as CO_2.

While there is a dearth of literature information on this issue for methanol oxidation, the work of Zum Mallen and Schmidt[4] on polycrystalline Rh at lower pressures offers a point of comparison. Specifically, we consider their rate data and kinetic modeling for an equimolar mixture of CH_3OH and O_2 at 0.2 Torr total pressure (presented in Figures 2b and 6a,c of ref 4). Figure 7B shows a plot of their observed CO selectivity and model-estimated CO coverage as a function of temperature. The relationship between these quantities is similar to that exhibited in Figure 7A, suggesting a common mechanism in these two pressure regimes.

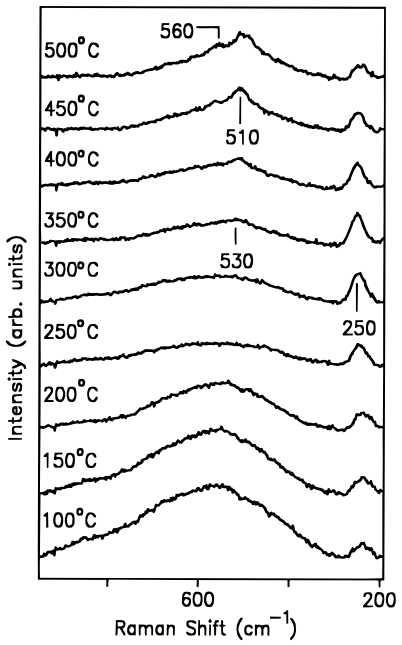

Figure 8. Temperature-dependent SER spectra obtained during exposure of Rh to 100 cm^3 min^{-1} of 80% O_2/17% Ar/3% CH_3OH at 1 atm total pressure. The spectral acquisition time was 20 s. See Figure 2 caption and text for further details.

Oxidation: Oxygen-Rich Conditions. Markedly different spectral results were obtained when employing reaction mixtures containing a large excess of oxygen. Figure 8 shows typical SER spectra acquired during heating a Rh surface in 100 cm^3 min^{-1} 80% O_2/3% MeOH/17% Ar at a total pressure of 1 atm. The spectrum obtained at 100 °C (bottom) shows a weak band at 250 cm^{-1}, along with a broad sloping baseline. Upon heating there was essentially no change until 250 °C, where the baseline diminished and the 250 cm^{-1} band intensity increased up to 350 °C before decreasing somewhat at higher temperatures. Additionally, traces of surface oxidation were observed by 350 °C, as evidenced by the appearance of a broad ca. 530 cm^{-1} feature (Figure 8). Further heating resulted in a more intense and well-defined oxide feature, revealing a sharper band at 510 cm^{-1} along with a shoulder at 560 cm^{-1} by 500 °C. Furthermore, this surface oxidation process was completely reversible upon cooling below 400 °C, the oxide features being removed.[14e]

An Arrhenius plot of corresponding rate measurements obtained by MS is presented in Figure 9. The only products formed under these conditions were CO_2 and H_2O (i.e., exhaustive methanol oxidation occurs), with reaction being detectable by 200 °C and exhibiting an activation energy of 7.5 ± 1 kcal mol^{-1} up to 350 °C. The carbon balance again closed to within 10%. Similar to the case of excess methanol (Figure 3), no significant temperature hysteresis in catalytic activity was observed, and the CO_2 formation rate became temperature-independent above 350 °C. To check whether the methanolic C−O bond also cleaves under reaction conditions, kinetic experiments were performed which involved substituting $^{18}O_2$ during the above experiment. This was in part prompted by our recent observation by SERS of CO dissociation on Rh.[14c] The isotope experiments revealed that *both* $C^{16}O^{18}O$ and $C^{18}O^{18}O$ form, with the latter species making up at least 25% of the observed CO_2 product. These results confirm *for the first time* that C−O bond cleavage is occurring on Rh during methanol oxidation. While no study of methanol oxidation on Rh reports this phenomenon, there is substantial evidence for this pathway on palladium[11d,24] and platinum,[25] although some

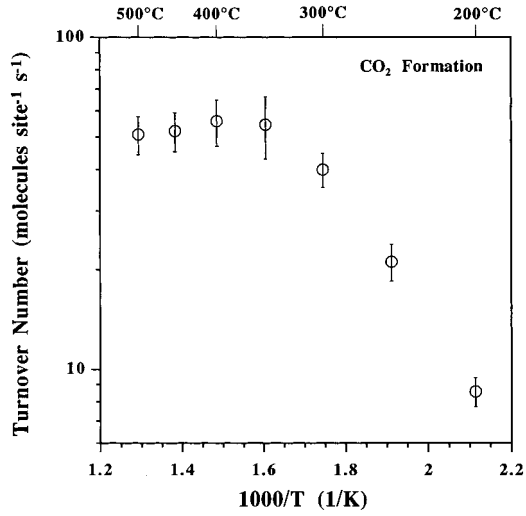

Figure 9. Arrhenius plot of CO_2 formation kinetics during exposure of Rh to 250 cm^3 min^{-1} of 80% O_2/17% Ar/3% CH_3OH at 1 atm total pressure. See Figure 2 caption and text for further details.

controversy still exists.[26] The observed catalyst deactivation during methanol dissociation (Figure 2), therefore, may at least in part be a result of surface carbon deposition from this process.

Methanol-Induced Oxide Removal. The observation of oxide formation during methanol oxidation, noted in Figure 8, encouraged us to investigate further the conditions for its formation and removal as well as a possible role in the catalytic reaction. The temperature at which the oxide begins to form (≈350 °C) under reaction conditions (Figure 8) is about 150 °C higher than in the case of pure oxygen,[13c] showing further that surface oxidation is suppressed by the presence of methanol. A likely explanation is that, rather than being incorporated into the Rh lattice, surface oxygen preferentially reacts with CH_3OH and its dissociation products. Significantly, the observed formation of CO_2 and H_2O at these temperatures (Figure 9) lends support to this supposition.

However, another interpretation is that the *oxide itself* might be an active intermediate or a supplier of oxygen for methanol oxidation. Given its stability at 200 °C in the presence of pure O_2, it is possible that some surface oxide is present in subdetectable levels at similar temperatures under reaction conditions. Furthermore, the temperature dependence of the extent of surface oxidation (Figure 8) and the reversibility of this process clearly indicate that Rh_2O_3, once formed, is reactive. Recent preliminary efforts[14d] at probing the reactivity of this oxide further bolster this claim. Transient SER spectral response experiments were performed which involved real-time monitoring of the reactive oxide removal by injection of pure methanol gas at various temperatures. Intriguingly, the oxide was seen to be removed extremely rapidly (within ca. 10 s) at around 350 °C, although a quantitative data analysis was thwarted by sluggish mixing characteristics of the flow reactor.[14d]

As noted above, however, recent reactor modifications have substantially diminished the reactor mixing time, prompting a more comprehensive study of methanol-induced oxide removal kinetics, as we now describe. After heating a Rh surface in 80% O_2/17% Ar/3% CH_3OH at 1 atm total pressure to 500 °C (cf. Figure 8, top spectrum), the reactor was flushed with pure Ar and the sample cooled to the desired reaction temperature. As the temperatures investigated are lower than those reported for thermal desorption of oxygen from Rh[16−18] and decomposition of Rh_2O_3,[19] this procedure resulted in a surface still covered by the oxide. Perhaps most importantly, the lack of any change

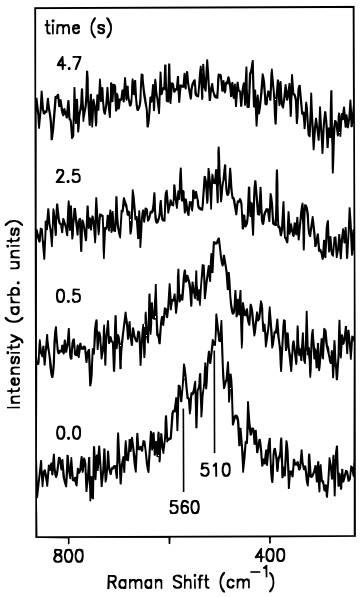

Figure 10. Transient SER spectra of an initially oxide-covered Rh surface at 350 °C following gas-phase switch from pure Ar to 1200 cm^3 min^{-1} 15% CH_3OH in Ar. The surface was previously heated in the fashion described for Figure 8 to 500 °C and the reactor flushed out with argon and cooled to the temperature of interest before methanol addition. The spectral acquisition time was 0.5 s.

in Raman intensity during this procedure confirmed that the oxide surface concentration was *identical with that observed during reaction*. The surface was subsequently exposed to 1200 cm^3 min^{-1} of 15% CH_3OH in Ar by rapid switching from the pure Ar gas flow. [Given the measured reactor residence time (3−4 s) for this flow rate, the composition of the reactor changes completely in ca. 10 s.]

Typical time-resolved SER spectra obtained at 350 °C following such a gas-flow switch are shown in Figure 10. Again, a spectral acquisition time of 0.5 s was utilized. At $t =$ 0 s (just prior to methanol introduction, bottom spectrum), the presence of surface oxide is clearly evidenced by the pair of features at 510 and 560 cm^{-1}. However, these bands began to disappear even within the first spectral acquisition period, with final removal achieved by 4−5 s. Identical experiments performed at lower temperatures revealed that the oxide removal rate was temperature-dependent at this methanol partial pressure, as illustrated by the temporal changes in the oxide coverage during the experiments at 200, 250, and 350 °C shown in Figure 11. These relative coverages are estimated by normalizing the integrated intensity of the 510/560 cm^{-1} bands at various times to its initial value, as for the case of CO above (Figure 7). Best-fit curves assuming a simple first-order dependence on oxide coverage are also included and discussed below.

To determine the dependence of the oxide removal kinetics on methanol pressure, gas flows containing 1.5% and 0.15% CH_3OH in Ar at 1 atm were also examined from 200 to 350 °C. In all cases the oxide removal appears to follow a first-order decay. Interestingly, however, the temperature dependence is markedly different than that observed at the highest methanol pressure (Figure 11). For example, Figure 12 shows the relative oxide coverage as a function of time during removal by 1.5% CH_3OH at 200, 250, 300, and 350 °C along with best-fit first-order decay curves. Significantly, the reaction rates are essentially *temperature-independent* from 250 to 350 °C, with only further lowering of the temperature to 200 °C resulting in an increased oxide removal time. Comparison of Figures 11 and 12 also reveals that the oxide removal rates for the two

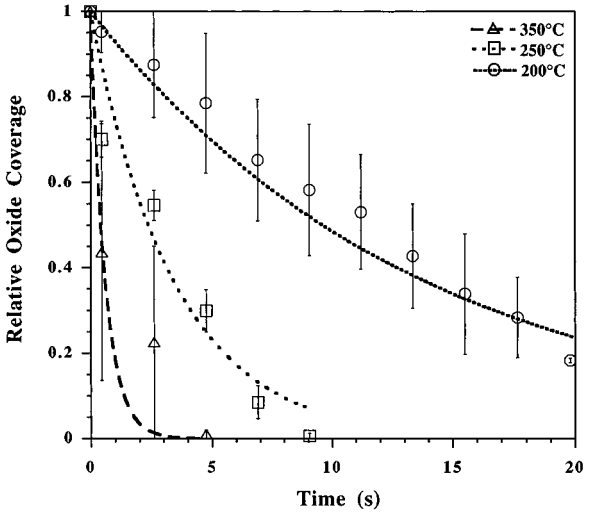

Figure 11. Plot of the Rh_2O_3 coverage as a function of time at 350 (triangles), 250 (squares), and 200 °C (circles) following the addition of 1200 cm^3 min^{-1} 15% CH_3OH in Ar at 1 atm. Coverages, as deduced from time-dependent SERS intensities as in Figure 10 (see text), are normalized to the maximum (i.e., initial) values. The corresponding curves represent best fits to a first-order rate law (see text).

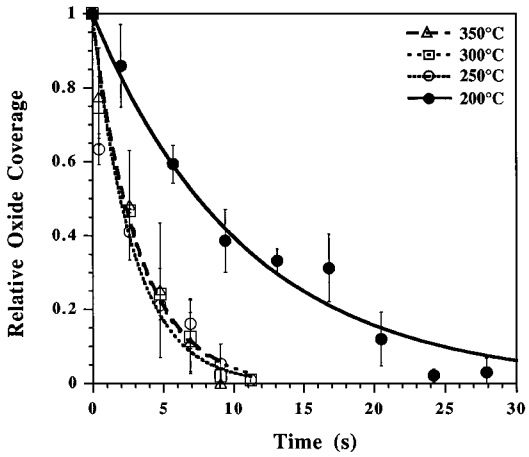

Figure 12. Plot of the Rh_2O_3 coverage as a function of time at 350 (triangles), 300 (squares), 250 (open circles), and 200 °C (black circles) following the addition of 1200 cm^3 min^{-1} 1.5% CH_3OH in Ar at 1 atm. Coverages, as deduced from time- dependent SERS intensities (see text), are normalized to the maximum (i.e., initial) values; also see Figure 11 caption.

pressure regimes become similar beginning at ca. 250 °C. Lowering the pressure another 10-fold to 0.15% CH_3OH not only results in further depression of the reaction rates but also yields temperature-independent kinetic behavior over essentially the entire range examined.

As alluded to above, the oxide removal rate exhibits an apparent first-order dependence on oxide concentration (Figures 11 and 12). Attempts to fit the data with second-order or nucleation/growth kinetics resulted in less satisfactory fits. Employing a simple first-order model to fit the oxide removal data allows the calculation of rate constants (s^{-1}) and activation energies for the process. (The fits for 15% and 1.5% CH_3OH are included in Figures 11 and 12, respectively.) Figure 13 shows the resulting Arrhenius plots for the three methanol pressures, revealing clearly the essentially temperature-independent behavior at the lower pressures. Note that the rates at the highest methanol pressure are strongly temperature-dependent, exhibiting an activation energy of 12 ± 2 kcal mol^{-1} with a preexponential factor of ca. 3.5×10^4 s^{-1}. Furthermore, the

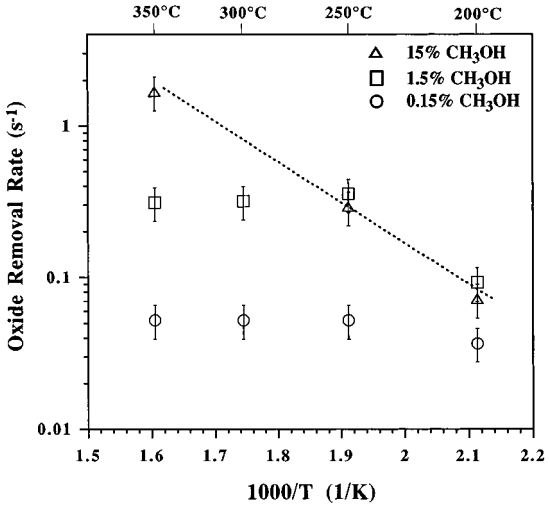

Figure 13. Arrhenius plot of oxide removal kinetics for 15% (triangles), 1.5% (squares), and 0.15% (circles) CH_3OH in argon. Rate constants (s^{-1}) were calculated by assuming a first-order dependence on oxide coverage and fitting the data (including those in Figures 10 and 11). The dashed line represents the boundary at which the rate-determining step of the process appears to change (see text).

convergence of the rates measured for the two lower methanol pressures at 250 °C and below suggests that this activated process again becomes prevalent. Taken together, these observations therefore suggest that a change in the rate-determining step (and/or mechanism) is occurring as the methanol pressure is raised and/or the temperature is lowered sufficiently. A boundary between these regimes is approximated by the dotted line in Figure 13.

Firm elucidation of the reaction mechanism is hampered by the lack of information regarding changes in adsorbed methanol, oxygen, and other species during the removal. Nevertheless, a simple pathway involving known surface processes is proposed here which qualitatively captures the observed behavior. The dependence of the rates on methanol partial pressure implies that the adsorption, desorption, and dissociation steps involving this moiety are of central importance. While it has been shown that adsorbed methanol first dissociates to surface methoxy,[6−10] it is well-known that the presence of adsorbed oxygen significantly affects this process.[7,10,11a] In a study of methanol adsorption on oxygen precovered Rh(111), for instance, Houtman and Barteau[7] showed that the dominant dissociation pathway involved abstraction of the methanolic hydrogen by oxygen.

Considering the probable steps involving Rh_2O_3 decomposition, a simple mechanistic sequence for oxide removal is proposed (S denotes a free site):

$$O^{2-} \leftrightarrow O_{(ads)} \quad (1)$$

$$CH_3OH_{(g)} + S \leftrightarrow CH_3OH_{(ads)} \quad (2)$$

$$CH_3OH_{(ads)} + O_{(ads)} \rightleftharpoons CH_3O_{(ads)} + OH_{(ads)} \quad (3)$$

The mechanism provides a framework for understanding the trends in oxide removal rates. At lower methanol pressures the removal rate is more likely to be controlled by the supply of the reductant "scavenger" (adsorbed methanol, as written, or a dissociated species), with steps 2 and/or 3 limiting the rate and step 1 remaining in quasi-equilibrium. This notion is not inconsistent with the essentially temperature-independent kinetics observed under these conditions (Figure 13). As the methanol pressure is raised, however, eventually step 3 should become sufficiently rapid so that adsorbed oxygen is efficiently removed. The rate would then become limited instead by the irreversible conversion of lattice oxide to adsorbed oxygen (step 1). It is the kinetics of this latter process, therefore, that is believed to be characterized by the dotted trace in Figure 13 and approached by the temperature-dependent rate data at the highest methanol pressure (triangles, Figure 13).

We have recently undertaken a related SERS examination of the transient reduction kinetics of rhodium oxide by gaseous hydrogen and carbon monoxide.[27] The results are of interest here since both adsorbed atomic hydrogen and CO may constitute the "oxide scavenger" species formed upon methanol adsorption. Interestingly, the initial oxide removal rates observed upon CO addition[27] are comparable to the maximum temperature-dependent rates obtained here in the presence of methanol. The rate law in oxide coverage at low temperatures ($\leq$250 °C) differs from the simple first-order behavior observed with methanol, the observed "autoinhibited" behavior due apparently to the buildup of high CO coverages detected by SERS. These findings are consistent with the involvement of CO as an active oxide scavenger in the methanol reaction given that insufficient CO is formed upon adsorption of the latter species to inhibit the oxide removal process. Considerably more facile reduction kinetics are observed in the presence of gaseous hydrogen in comparison to either methanol or CO. The former also display an induction time prior to extremely rapid oxide removal.[27] These observed kinetics suggest that the hydrogen reductant is able to circumvent the need for step 1 prior to oxygen removal.[27] In any case, the markedly different kinetics observed in the presence of methanol suggests that hydrogen atoms do not constitute the predominant oxygen scavenger in the former process.

While several specific mechanistic questions remain unanswered, it is interesting to consider now whether the rates of the methanol-induced oxide-removal process are comparable with methanol oxidation under excess oxygen conditions (Figure 9). (This circumstance would be necessary for the process to be a candidate for the rate-determining step for methanol oxidation.) It is difficult to make a clear-cut comparison given the changes in methanol pressure during the removal experiments and the presence of oxygen gas during the steady-state reaction. Nevertheless, the transient experiments using 15% CH_3OH in Ar (Figure 11) likely offer the best comparisons in that oxide removal during reaction probably occurs in the above-described "activated regime". First, we estimate the amount of oxide (Rh_2O_3) in our thin film at 500 °C under excess oxygen reaction conditions to be ca. 5×10^{15} O^{2-} (corresponding to approximately 50% of rhodium atoms oxidized). This estimate is made by comparing such surfaces to one heated in pure O_2. Next, the coverage of oxide at 350 °C under the same conditions is estimated from the intensities in Figure 8 to be around 10% of this value, or 5×10^{14} O^{2-}. Using the rate constant obtained above for 350 °C in the activated regime (1.7 s^{-1}, Figure 13), the oxide removal rate under reaction conditions is estimated to be ca. 8×10^{14} O^{2-} s^{-1} or, as stated in turnover frequency, ca. 0.5 O^{2-} $site^{-1}$ s^{-1}. In order for this surface process to be the rate-determining step in methanol oxidation, the rate should be comparable to that observed for steady-state CO_2 formation. However, Figure 9 reveals that the CO_2 (i.e., CH_3OH) turnover frequency is approximately 2 orders of magnitude higher ($\approx$50 molecules $site^{-1}$ s^{-1}). Moreover, assuming a higher oxide coverage at 350 °C still results in estimated rates that are significantly lower than this measured value. The analysis

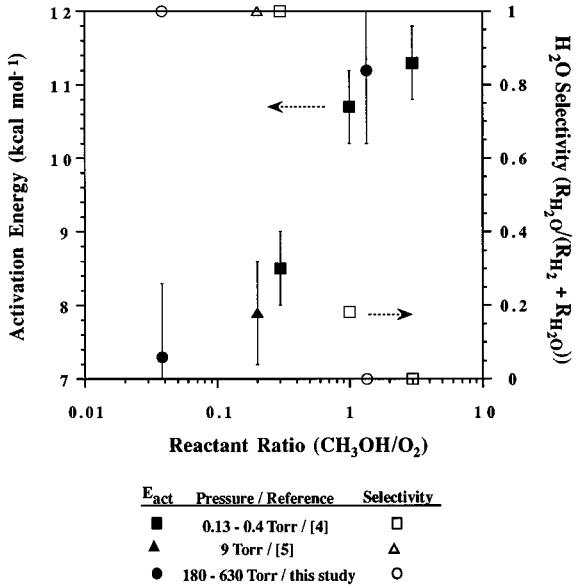

Figure 14. Plot of apparent activation energy for methanol oxidation (solid symbols) and fractional selectivity toward H_2O production (open symbols) as a function of reactant ratio (CH_3OH/O_2) over a wide range of total pressures (0.13−630 Torr). Data were obtained from ref 4 (squares), ref 5 (triangles), and the present study (circles). See text for details.

therefore suggests that the oxide itself is most likely not a major reaction intermediate. Further corroborating evidence is the difference between the activation energy for CO_2 formation (7.5 ± 1 kcal mol^{-1}) and that for oxide removal (12 ± 2 kcal mol^{-1}).

Overall Mechanisms. While the required kinetic data are sparse, it is appropriate to consider briefly the mechanistic differences between methanol oxidation in the absence and presence of excess oxygen. The observed variations in reaction product selectivity at the reactant molar ratios examined indicate the occurrence of the following three overall reactions:

$$CH_3OH_{(g)} \rightarrow CO_{(g)} + 2H_{2(g)} \quad (4)$$

$$CH_3OH_{(g)} + {}^1/_2O_{2(g)} \rightarrow CO_{2(g)} + 2H_{2(g)} \quad (5)$$

$$CH_3OH_{(g)} + {}^3/_2O_{2(g)} \rightarrow CO_{2(g)} + 2H_2O_{(g)} \quad (6)$$

For a molar excess of methanol, a combination of reactions 4 and 5 is occurring as evidenced by the formation of CO, CO_2, and H_2. In contrast, the exhaustive oxidation (reaction 6) is, not surprisingly, dominant under excess oxygen conditions.

Some insight regarding the mechanistic nature of the oxidative reactions 5 and 6 may be gleaned by comparing the apparent overall activation energies, E_a, for methanol oxidation to form CO_2 in the methanol- and oxygen-rich cases (Figures 4 and 9, respectively). The former value is significantly higher, 12 versus 7.5 kcal mol^{-1}. Interestingly, a similar variation in E_a values with the CH_3OH/O_2 molar ratio is seen for literature data, as shown collectively in Figure 14 (filled symbols). Also included in Figure 14 are values of the selectivity toward formation of H_2O rather than H_2, plotted on the same *x*-axis (open symbols). The fractional H_2O selectivity is seen to drop qualitatively, from 1.0 to 0, as the CH_3OH/O_2 ratio is increased above unity (Figure 14).

These changes can be rationalized most simply by asserting that methanol adsorption to form adsorbed CO (or a partial oxidation fragment) is rate-determining. This rests on the notion that the coverage (or even presence) of adsorbed oxygen will be higher in the oxygen-rich case, creating the possibility for "oxygen-assisted" methanol decomposition involving H atom transfer from the methanol hydroxyl group.[7,10] The oxygen-assisted pathway not only is known to facilitate H_2O production[7,10] but also might be expected to involve a smaller activation energy as compared to methanol decomposition involving hydrogen transfer to a bare metal site. These expectations are in harmony with the observations (Figure 14).

Concluding Remarks

While limited somewhat by the ability to deduce firmly the identity as well as coverage of adsorbates with vibrational spectroscopy, we believe that the foregoing affords new insight into the surface chemical factors that control the kinetics and mechanisms of this important catalytic oxidation process. The acquisition of real-time surface vibrational information under ambient-pressure flow-reactor conditions, a unique feature of the present approach, uncovers the ability of the catalyst to operate efficiently in the presence of high coverages of oxygenated species. Perhaps most striking is the observed presence of substantial amounts of rhodium oxide (Rh_2O_3) under oxygen-rich reaction conditions that can nonetheless undergo reaction extremely rapidly (≤1 s) with adsorbed methanol rather than merely act as a catalytic inhibitor. (As discussed elsewhere,[14e] a dramatically different situation applies to oxides formed on Pd under similar conditions.) This facile reactivity of even the lattice oxide can readily account for the efficient performance of the rhodium catalyst despite its penchant for extensive surface oxidation. Oxygen plays an important role in the surface chemistry even under methanol-rich reaction conditions, as evidenced clearly by the substantial production of adsorbed CO, which is not detected upon methanol dissociation in its absence. This surface process may well involve facilitating methanol dissociation by hydrogen transfer to juxtaposed atomic oxygen (cf. last section). While only a portion of the adsorbed CO appears to play a direct catalytic role, its thermal stability is substantially greater than for adsorbate formed by direct gas-phase CO dosing, presumably reflecting the importance of coadsorbates.

Overall, then, the potent catalytic properties of rhodium toward methanol oxidation even at higher pressures appears to arise from the ability of adsorbed oxygen (and oxide) present to *both* efficiently dissociate methanol and react with the resultant carbon-containing adsorbed fragments. This hallmark of rhodium is highlighted further by the presence of a CO_2 formation pathway via oxidation of adsorbed carbon produced by C−O bond scission, as deduced by $^{18}O_2$ kinetic measurements.

Consequently, we feel justified in asserting that our utilization of Raman spectroscopy with SERS-active transition-metal film surfaces can contribute importantly to the understanding of surface catalytic chemistry over a uniquely expansive range of gas-phase (and liquid) environments. Exploitation of these tactics to interrogate a widening array of surface environments and catalytic processes is underway in our laboratories.

Acknowledgment. This work was supported by a grant to C.G.T. and M.J.W. (CTS-9312008) from the National Science Foundation. Steven Schwallie is thanked for assistance with the kinetic measurements. We acknowledge the Dow Chemical Company for financing the Advanced Instrumentation Labora-

tory in the School of Chemical Engineering at Purdue, which was utilized for the MS kinetic experiments.

References and Notes

(1) Spivey, J. J. *Ind. Eng. Chem. Res.* **1987**, *26*, 2165.

(2) For example: Bailey, R. A.; Clark, E. M.; Ferris, J. P.; Krause, S.; Strong, R. L. *Chemistry of the Environment*; Academic Press: New York, 1978.

(3) Papapolymerou, G. A.; Schmidt, L. D. *Langmuir* **1987**, *3*, 1098.

(4) Zum Mallen, M. P.; Schmidt, L. D. *J. Catal.* **1996**, *161*, 230.

(5) McCabe, R. W.; Mitchell, P. J. *Appl. Catal.* **1986**, *27*, 83.

(6) Parmeter, J. E.; Jiang, X.; Goodman, D. W. *Surf. Sci.* **1990**, *240*, 85.

(7) Houtman, C.; Barteau, M. A. *Langmuir* **1990**, *6*, 1558.

(8) Kruse, N.; Chuah, G.-K.; Abend, G.; Cocke, D. L.; Block, J. H. *Surf. Sci.* **1987**, *189/190*, 832.

(9) Solymosi, F.; Berko, A.; Tarnoczi, T. I. *Surf. Sci.* **1984**, *141*, 533.

(10) Solymosi, F.; Tarnoczi, T. I.; Berko, A. *J. Phys. Chem.* **1984**, *88*, 6170.

(11) (a) Davis, J. L.; Barteau, M. A. *Surf. Sci.* **1988**, *197*, 123. (b) Davis, J. L.; Barteau, M. A. *Surf. Sci.* **1987**, *187*, 387. (c) Solymosi, F.; Berko, A.; Toth, Z. *Surf. Sci.* **1993**, *285*, 197. (d) Chen, J.-J.; Jiang, Z.-C.; Zhou, Y.; Chakraborty, B. R.; Winograd, N. *Surf. Sci.* **1995**, *328*, 248.

(12) (a) Wilke, T.; Gao, X; Takoudis, C. G.; Weaver, M. J. *Langmuir* **1991**, *7*, 714. (b) Wilke, T.; Gao, X.; Takoudis, C. G.; Weaver, M. J. *J. Catal.* **1991**, *130*, 62.

(13) (a) Tolia, A.; Wilke, T.; Weaver, M. J.; Takoudis, C. G. *Chem. Eng. Sci.* **1992**, *47*, 2781. (b) Tolia, A. A.; Weaver, M. J.; Takoudis, C. G. *J. Vac. Sci. Technol. A* **1992**, *11 (4)*, 2013. (c) Tolia, A. A.; Smiley, R. J.; Delgass, W. N.; Takoudis, C. G.; Weaver, M. J. *J. Catal.* **1994**, *150*, 56. (d) Tolia, A. A.; Williams, C. T.; Takoudis, C. G.; Weaver, M. J. *J. Phys. Chem.* **1995**, *99*, 4599. (e) Tolia, A. A.; Williams, C. T.; Weaver, M. J.; Takoudis, C. G. *Langmuir* **1995**, *11*, 3438.

(14) (a) Williams, C. T.; Tolia, A. A.; Weaver, M. J.; Takoudis, C. G. *Chem. Eng. Sci.* **1996**, ***51***, 1673. (b) Williams, C. T.; Tolia, A. A.; Chan, H. Y. H.; Takoudis, C. G.; Weaver, M. J. *J. Catal.* **1996**, *163*, 63. (c) Williams, C. T.; Black, C. A.; Weaver, M. J.; Takoudis, C. G. *J. Phys. Chem. B* **1997**, *101*, 28. (d) Williams, C. T.; Takoudis, C. G.; Weaver, M. J. *J. Catal.* **1997**, *170*, 207. (e) Chan, H. Y. H.; Williams, C. T.; Weaver, M. J.; Takoudis, C. G. *J. Catal.*, in press.

(15) (a) Gao, P.; Gosztola, D.; Leung, L.-W. H.; Weaver, M. J. *J. Electroanal. Chem.* **1987**, *233*, 211. (b) Leung, L.-W. H.; Weaver, M. J. *J. Am. Chem. Soc.* **1987**, *109*, 5113. (c) Leung, L.-W. H.; Weaver, M. J. *Langmuir* **1988**, *4*, 1076.

(16) Fisher, G. B.; Schmieg, S. J. J. *Vac. Sci. Technol. A* **1983**, *1*, 1064.

(17) Thiel, P. A.; Yates, J. T., Jr.; Weinberg, W. H. *Surf. Sci.* **1979**, *82*, 22.

(18) Castner, D. G.; Somorjai, G. A. *Appl. Surf. Sci.* **1980**, *6*, 29.

(19) (a) Kellogg, G. L. *Phys. Rev. Lett.* **1985**, *54*, 82. (b) Kellogg, G. L. *J. Catal.* **1985**, *92*, 167. (c) Kellogg, G. L. *Surf. Sci.* **1986**, *171*, 359.

(20) (a) Thiel, P. A; Williams, E. D.; Yates, J. T., Jr.; Weinberg, W. H. *Surf. Sci.* **1979**, *84*, 54. (b) Castner, D. G.; Somorjai, G. A. *Surf. Sci.* **1979**, *83*, 60.

(21) (a) Weaver, M. J.; Corrigan, D. S.; Gao, P.; Gosztola, D.; Leung, L.-W. H. *ACS Symp. Ser.* **1988**, *378*, 303. (b) Weaver, M. J.; Hupp, J. T.; Barz, F.; Gordon, J. G.; Philpott, M. R. *J. Electroanal. Chem.* **1984**, *160*, 321.

(22) Zum Mallen, M. P.; Williams, W. R.; Schmidt, L. D. *J. Phys. Chem.* **1993**, *97*, 625.

(23) See for example: Campbell, C. T.; Shi, S. K.; White, J. M. *J. Phys. Chem.* **1979**, *83*, 3, 2255.

(24) Levis, R. J.; Jiang, Z.; Winograd, N. *J. Am. Chem. Soc.* **1988**, *110*, 4431.

(25) Wang, J.; Masel, R. I. *J. Catal.* **1990**, *126*, 519.

(26) Guo, X.; Hanley, L.; Yates, Jr., J. T. *J. Am. Chem. Soc.* **1989**, *111*, 3155.

(27) Williams, C. T.; Chen, E. K.-Y.; Takoudis, C. G.; Weaver, M. J., submitted to *J. Am. Chem. Soc.*